Elsevier required licence: © <2020>. This manuscript version is made available under the CC-BY-NC-ND 4.0 license http://creativecommons.org/licenses/by-nc-nd/4.0/
The definitive publisher version is available online at https://doi.org/10.1016/j.jmmm.2020.167290

A Generalized Inverse Preisach Dynamic Hysteresis Model of Fe-Based Amorphous Magnetic Materials

Pejush Chandra Sarker*[a], Youguang Guo[a], Hai Yan Lu[a], Jian Guo Zhu[b]

[a] Faculty of Engineering and Information Technology, University of Technology Sydney, Australia
[b] School of Electrical and Information Engineering, The University of Sydney, Australia

Abstract

Fe-based amorphous magnetic materials are attracting more and more attentions in the application of low and medium frequency transformers due to their favorable properties of low core loss and high saturation magnetic flux density. Accurate modelling of their static and dynamic characteristics is required for analysis and design optimization of low and medium frequency transformers. In particular, for numerical analysis using the vectorial magnetic potential, an inverse magnetic hysteresis model is needed to predict the magnetic field strength from the magnetic flux density. When the excitation varies with time, the magnetic hysteresis model must be able to predict the dynamic hysteresis characteristics. This paper presents a generalized inverse Preisach dynamic hysteresis model for dynamic characterization of Fe-based magnetic materials. This model incorporates the reversible magnetization and magnetization dependent hysteresis, as well as all core loss components, including the hysteresis, eddy current, and excess losses. The proposed model can predict accurately the magnetic field strength from the magnetic flux density and hence accurate core losses. The predicted results are verified by experimental measurements.

Keywords— Preisach model; Inverse Preisach model; Fe-based amorphous magnetic material; Hysteresis and dynamic losses

1. Introduction

In the last few decades, it has always been highly desirable to design electromagnetic devices of small size, low weight, and high efficiency in energy conversion systems. The solid-state transformer (SST), which integrates medium or high frequency transformers together with pulse-width-switching power electronic converters, has attracted great attentions due to its high-power density, which is mainly achieved by using magnetic cores of low core losses and high saturation magnetic flux density [1]. The dry type transformers in both the SST and conventional energy conversion systems are presently preferred to avoid the periodic change of dielectric liquid used for cooling and insulation purposes.

In a transformer, the core material is one of the prime factors that determine the performance since the core loss highly affects the power efficiency and density. Because the power density depends on the power losses and saturation magnetic flux density, the core material selection is one of the key factors in the design of SST and conventional transformers. Among the commonly used core materials, such as silicon sheet steels (SiFe), amorphous alloys, nanocrystalline ribbons and soft ferrites, the SiFe is a magnetic material widely used in the conventional low frequency transformers due to its availability, low cost and high saturation flux density. For instance, the saturation flux density of SiFe 10JNHF600 is 1.87 T [2]. On the other hand, soft ferrites are mostly utilized in high frequency SST because of its very low core loss. The core loss of ferrite 3C85 at 100 kHz and 0.1 T is 0.009 kW/kg, which is much lower than 0.24 kW/kg of SiFe 10JNHF600 under the same condition [2]. The main drawback of soft ferrites is its low saturation magnetic flux density (B_s), e.g. 0.45 T for 3C85. Recently, the amorphous and nanocrystalline magnetic materials have attracted increasing attentions due to their features of high electrical resistivity, high permeability, and low power loss. Because of their very thin foil structures and high resistivities, the eddy current and excess losses, two key core loss components (the other is the hysteresis loss), are significantly lower than those of SiFe. However, the high manufacturing cost and low magnetic saturation flux density (about 1.20 T) of nanocrystalline magnetic materials hinders its applications in low and medium frequency transformers. This makes Fe-based amorphous magnetic materials a favourable candidate of core materials for low and medium frequency transformers. They are attracting more and more interests in the last decade because of their relatively high saturation magnetic flux densities, between 1.41 T and 1.64 T depending on the chemical compositions [3], which is higher than those of nanocrystalline and soft ferrite materials, and lower core loss than SiFe. Hitachi Metals Ltd. produces a few types of Fe-based amorphous materials, such as Metglas 2605SA1 (B_s = 1.41 T) and Metglas 2605S3A (B_s = 1.56 T), and Henan ZY Amorphous Technology Co. Ltd. produces a Fe-based amorphous magnetic material known as Zhongyue amorphous j1k101 (B_s = 1.56 T) [4,5]. In this paper, the Zhongyue amorphous j1k101 alloy is studied.

*Corresponding author
Email: pejushchandra.sarker@student.uts.edu.au

Characterization of magnetic core materials is very important for design of transformers. There are mainly two types of methods for core loss prediction, i.e. the empirical methods and macroscopic methods. The empirical methods are based on the Steinmetz equation where the Steinmetz parameters are calculated by curve fitting experimental measurement data at different frequencies and magnetic flux densities [6]. In [7], Fe-based amorphous magnetic materials (Metglas 2605S3A and 2605SA1) were characterized by the empirical method. The empirical methods generate higher error if the loss is predicted at a point (frequency and magnetic flux density) far from those used for calculating the Steinmetz parameters. Neither they can predict the trajectories of magnetic flux density versus magnetic field strength. Under the non-sinusoidal excitations generated by power electronic converters, the harmonic contents would generate significant core losses due to the presence of minor loops [8]. The empirical methods cannot cope with the minor loops in the non-sinusoidal magnetization process.

On the other hand, the macroscopic methods, such as the Preisach and Jiles-Atherton (J-A) models, can predict the core losses by tracing explicitly the magnetization trajectory of magnetic flux density versus magnetic field strength [9–11]. For non-sinusoidal excitation, the Preisach model can provide better results compared to the J-A model [12].

The Preisach model is used in this study to characterize the amorphous material as the operating magnetic flux density is generally higher than the remanent flux density, which is required to achieve high power density. Compared with the normal Preisach model which considers a magnetization independent process, the moving Preisach model [13–18] deals with a magnetization dependent process by introducing a feedback coefficient. Although this feedback coefficient changes with the magnitude of flux density and magnetic field strength, a constant feedback coefficient can be used to obtain adequate effects [15]. In the magnetization process of a ferro-magnetic material, there exist two magnetization components: the reversible and irreversible magnetization components [19]. However, both the normal and moving Preisach models consider only the irreversible magnetization component. The generalized Preisach model, on the other hand, takes into account both the irreversible and reversible magnetization components, as well as the magnetization dependent component with a feedback coefficient [20–22].

The classical Preisach model is generally used for predicting the static hysteresis loss where the Preisach function is a static function of magnetic field strength. For prediction of dynamic hysteresis loss (a combination of hysteresis, eddy current and excess losses), dynamic Preisach models can be used where the Preisach function considers not only the magnetic field strength but also the change rate of magnetic flux density with respect to time [17,23].

For design and performance analysis of electromagnetic devices and systems, the finite element method is commonly employed to calculate the magnetic field distribution by using the vectorial magnetic potential, which requires the prediction of magnetic field strength from the magnetic flux density in each finite element. Since the normal Preisach models predict magnetic flux density from field strength, an inverse Preisach is required for this case. In [24], a dynamic inverse Preisach model was proposed, in which the inverse Preisach function is obtained by curve fitting the first order polynomial function of static inverse Preisach function and the rate of change of magnetic flux density with time. In [25], another inverse Preisach method was proposed based on the recursive procedure which has high computational burden. In [11], a normal inverse Preisach model was presented by using the normal Preisach function to find out the magnetic field strength from the magnetic flux density. The advantage of normal inverse method in [11] is that it does not require any iteration and extra curve fitting so that the computational cost is kept low. However, none of the above mentioned inverse Preisach models consider the reversible magnetization and feedback coefficient in the magnetization process. In addition, to the best knowledge of authors, no investigation has been reported in the literature on the effects of minor loops on characterization process using the inverse Preisach models. Neither has the normal or inverse Preisach models been used to characterize the Fe-based amorphous magnetic material, in particular Zhongyue amorphous j1k101 [5].

This study aims to characterize the hysteretic effects of Fe-Based amorphous materials using the normal and inverse Preisach models. The key contributions are: (i) Characterization of the static hysteretic effects of selected Fe-based amorphous magnetic materials by the normal and inverse Preisach models; (ii) Calculation of total core loss of Fe-based amorphous magnetic materials by the proposed inverse dynamic Preisach model which incorporates hysteresis, eddy current and excess losses; (iii) Development of a generalized inverse Preisach model based on the generalized Preisach model by incorporating the reversible magnetization and magnetization dependent hysteresis effects; (iv) Development of a new technique to find out the feedback coefficient of the generalized Preisach model whose value varies with the magnitude of magnetic flux density; (v) Investigation of the effects of minor loops by using the proposed inverse Preisach model. The proposed methods are validated by substantial agreement between simulation and experimental results.

The rest of the paper is organised as follows: Section 2 reviews the normal Preisach model, followed by a review of the generalized Preisach model. An inverse Preisach model is proposed in Section 3. Section 4 presents the implementation of Preisach model for Fe-Based amorphous materials, followed by the implementation of

inverse Preisach model in Section 5. Section 6 presents the incorporation of dynamic effects in the Preisach models. Section 7 shows the experimental validations of proposed techniques and models. Section 8 concludes the paper and shed light on a few future works.

2. Review of Preisach Model

2.1. Normal Preisach Model

In the normal Preisach model, it is assumed that a magnetic material consists of a set of magnetic dipoles [26], each of which has rectangular elementary shapes as shown in Fig. 1(a) where two switching magnetic field strengths, denoted by α and β, are considered in the increasing and decreasing magnetic trajectories respectively. Fig. 1(b) shows the Preisach diagram, where S is the triangular region on the (α, β) plane for $H_{sat} \geq \alpha \geq \beta \geq -H_{sat}$, and S^+ and S^- are regions of positive and negative switched dipoles. If the applied magnetic field strength is H, the output magnetization M and the corresponding magnetic flux density B can be calculated by (1) and (2) [27,28] as follows, respectively.

$$M(H) = \int_S \mu(\alpha, \beta)\gamma_{\alpha\beta}(H)\, d\alpha\, d\beta \tag{1}$$

$$B = \mu_0[H + M(H)] \tag{2}$$

where $\mu(\alpha, \beta)$ is the distribution function of the magnetic dipoles, $\gamma_{\alpha\beta}$ the Preisach operator which is 1 on S^+ and -1 on S^-, and S the triangular region on the (α, β) plane for $H_{sat} \geq \alpha \geq \beta \geq -H_{sat}$ as shown in Fig. 1(b).

From the Preisach diagram shown in Fig. 1(b), the downward and upward magnetizations for a given magnetic field strength can be expressed as

$$M(H) = M(H_n) - 2T(H_n, H) \qquad \text{(Downward)} \tag{3}$$

$$M(H) = M(H_n) + 2T(H, H_n) \qquad \text{(Upward)} \tag{4}$$

where H_n represents the magnetic field strength at the last reversal point and $T(\alpha, \beta)$ is a function of the upward and downward magnetization trajectories. $T(\alpha, \beta)$ can be calculated from a data table of the limiting hysteresis loop, i.e. the largest loop of B (magnetic flux density) and H (magnetic field strength) of a given magnetic core measured at a very low frequency (e.g. lower than 1 Hz), by [27,28]

$$T(\alpha, \beta) = \frac{M_u(\alpha) - M_d(\beta)}{2} + F(\alpha)F(-\beta) \tag{5}$$

where $M_d(\alpha)$ and $M_u(\beta)$ are the downward and upward magnetizations of the limiting loop, and $F(\alpha)$ and $F(-\beta)$ can be determined by

$$F(\alpha) = \frac{M_d(\alpha) - M_u(\alpha)}{2\sqrt{M_d(\alpha)}} \quad \text{when } \alpha \geq 0 \tag{6}$$

$$F(\alpha) = \sqrt{M_d(-\alpha)} \qquad \text{when } \alpha < 0. \tag{7}$$

The initial magnetization can be expressed as

$$M(H) = T(H, -H) \tag{8}$$

2.2. Generalized Preisach Model

In the generalized Preisach model, the irreversible component of magnetization is obtained by using the normal Preisach model and the reversible component is proportional to the difference between the anhysteretic magnetization and irreversible magnetization components [22]. To make the magnetization dependent Preisach function, a magnetization feedback is added in the Preisach model. The combination of applied magnetic field strength and feedback magnetic field strength is generally known as effective magnetic field strength [15]. Therefore, the magnetization of a magnetic material, and the corresponding reversible magnetization and effective magnetic field strength at a given magnetic field strength can be written as [10,22]

$$M(H) = M_{irr}(H_e) + M_{rev}(H_e) \tag{9}$$

$$M_{rev}(H_e) = Q\{M_{anh}(H_e) - M_{irr}(H_e)\} \tag{10}$$

$$H_e = H + KM \tag{11}$$

where M_{irr} is the irreversible magnetization, M_{rev} the reversible magnetization, M_{anh} the anhysteric magnetization, H_e the effective magnetic field strength, K the feedback coefficient, and Q a constant.

Substituting (10) into (9), one obtains

$$M(H) = \mathrm{S}M_{irr}(H_e) + (1-\mathrm{S})M_{anh}(H_e) \tag{12}$$

where S=1–Q is known as the squareness of the elementary loop which can be calculated using the initial susceptibilities of normal magnetization and anhysteretic magnetization [22]. Since there is a feedback coefficient in the generalized Preisach models, an iterative process is needed to calculate the magnetization at each point of the applied magnetic field strength.

3. Inverse Preisach Model

3.1. Normal Inverse Preisach Model

The normal inverse Preisach model, based on the above mentioned normal Preisach model, calculates the magnetic field strength from the magnetic flux density [11]. The prediction of the magnetic field strength for the next time step can be obtained by [10].

$$H(t+\Delta t) = H(t) + \frac{\Delta B}{dB/dH} \tag{13}$$

where ΔB is the change of magnetic field density between two successive discrete times, Δt the time step, and dB/dH the derivative of magnetic flux density B with respect to magnetic field strength H.

Taking the first order derivative of both sides of (2) with respective to H, one obtains

$$\frac{dB}{dH} = \mu_0 + \mu_0 \frac{dM}{dH} \tag{14}$$

where dM/dH can be obtained from the limiting loop and the magnetic flux density.

Since the corresponding upward and downward magnetizations are known for a given limiting loop, the derivatives of the upward and downward magnetizations, dM_d/dH and dM_u/dH, of the limiting loop with respect to H can be obtained. Consequently, the first order derivatives of upward and downward magnetizations with respect to H can be calculated from (3) and (4) by

$$\frac{dM}{dH} = -2\frac{dT(H_n, H)}{dH} \quad \text{For downward trajectory} \tag{15}$$

$$\frac{dM}{dH} = 2\frac{dT(H, H_n)}{dH} \quad \text{For upward trajectory} \tag{16}$$

where $dT(H_n, H)/dH$ and $dT(H, H_n)/dH$ can be calculated from (5) by

$$\frac{dT(H_n, H)}{dH} = -\frac{1}{2}\frac{dM_d}{dH} - F(H_n)\frac{dF(-H)}{dH} \tag{17}$$

$$\frac{dT(H, H_n)}{dH} = \frac{1}{2}\frac{dM_u}{dH} + F(-H_n)\frac{dF(H)}{dH} \tag{18}$$

Similarly, the initial magnetization dM/dH can be obtained from (8) by

$$\begin{aligned}\frac{dM}{dH} &= \frac{dT(H, -H)}{dH} \\ &= \frac{1}{2}\frac{dM_u(H)}{dH} + \frac{1}{2}\frac{dM_d(-H)}{dH} + 2F(H)\frac{dF(H)}{dH}\end{aligned} \tag{19}$$

where $dF(H)/dH$ can be obtained from (6) and (7) by

$$\frac{dF(H)}{dH} = \frac{1}{4\sqrt{M_d(H)}}\frac{dM_d}{dH}\left\{1 + \frac{M_u}{M_d}\right\} - \frac{1}{2\sqrt{M_d(H)}}\frac{dM_u}{dH} \quad \text{for } H \geq 0 \tag{20}$$

$$\frac{dF(H)}{dH} = -\frac{1}{2\sqrt{M_d(-H)}}\frac{dM_d(-H)}{dH} \qquad \text{for } H < 0. \tag{21}$$

3.2. The Proposed Inverse Preisach Model

The inverse Preisach model proposed in this paper is derived from the generalized Priesach model presented in Section *2.2* by replacing the magnetic field strength with the effective magnetic field strength. While the magnetic field strength is calculated by (13), similar to the normal inverse Preisach model, the proposed inverse Preisach model is different from the normal inverse Preisach in the way to calculate dB/dH in (13). The first order derivative of the effective field strength with respect to the applied magnetic field strength (dH_e/dH) can be obtained from (11) by

$$\frac{dH_e}{dH} = 1 + K\frac{dM}{dH} \tag{22}$$

and

$$\frac{dM}{dH} = \frac{dM}{dH_e}\frac{dH_e}{dH}. \tag{23}$$

Substituting (22) into (23), one obtains

$$\frac{dM}{dH} = \frac{\dfrac{dM}{dH_e}}{1 - K\dfrac{dM}{dH_e}}. \tag{24}$$

The first order derivative of magnetization with respect to the effective magnetic field strength (dM/dH_e) can be obtained from (12) by

$$\frac{dM}{dH_e} = \mathrm{S}\frac{dM_{irr}}{dH_e} + (1-\mathrm{S})\frac{dM_{anh}}{dH_e} \tag{25}$$

where dM_{irr}/dH_e can be calculated by using the normal inverse Preisach model and dM_{anh}/dH_e can be obtained from the anhysteretic curve.

Substituting (24) into (14), one obtains

$$\frac{dB}{dH} = \mu_0 + \mu_0\frac{\dfrac{dM}{dH_e}}{1 - K\dfrac{dM}{dH_e}} \tag{26}$$

It is worth noting that the proposed inverse Preisach model does not require an iteration process although the generalized Preisach model does.

4. Implementation of Preisach Models

This section presents the implementation of the normal and generalized Preisach models, which require only the limiting loop data, and take the magnetic field strength as the input. Fig. 2 shows the measured limiting loop of Fe-based amorphous magnetic material, Zhongyue amorphous j1k101, where the left and right trajectories are the downward and upward trajectories of the limiting loop, and the remanence and coercive force are 0.81 T and 10.8 A/m, respectively. Because of the symmetry, only the left half of the limiting loop is stored in the form of a look up table.

4.1. Implementation of Normal Preisach Model

In the normal Preisach model, the initial magnetization at a given magnetic field strength is calculated by (8). After reaching the first reversible point, the operating point is at the downward trajectory as shown in Fig. 3. For the downward and upward trajectories, the magnetizations at a given magnetic field strength are calculated by (3) and (4), respectively. The magnetisation and corresponding magnetic field strength at the last reversible point are stored as they are required in (3) and (4). The process is repeated until it reaches the final time step. Finally, the associated magnetic flux density B can be obtained by (2).

4.2. Implementation of Generalized Preisach Model

To implement the generalized Preisach model, the anhysteretic curve, squareness and feedback coefficient are required for a given magnetic material. The anhysteric magnetization is calculated by using the normal Preisach model where an AC magnetic field strength is superimposed on a DC magnetic field strength at each point [22,28], and the amplitude of AC magnetic field strength is set to decay gradually from the maximum to zero to simulate the demagnetization process. The anhysteric magnetization and its derivative of the Fe-based amorphous material sample are shown in Fig. 4, which are used to identify the squareness and feedback coefficient, as shown in the following subsections.

4.2.1. Identification of Squareness

The squareness, S, can be calculated by [22]

$$S = 1 - \frac{\chi_{io}}{\chi_{anho}} \tag{27}$$

where χ_{io} and χ_{anho} are the initial susceptibilities of the normal and anhysteretic magnetization curves respectively.

4.2.2. Identification of Feedback Coefficient

According to [15], the the magnetization feedback coefficient K can be calculated by

$$K = \frac{M_e - M}{\chi M} \tag{28}$$

where M and M_e are the magnetizations calculated by the normal Preisach model and measured by experiment respectively, and χ is the susceptibility of a major loop at a given magnetic field strength.

Fig. 5 illustrates the feedback coefficient values for the upward magnetization of the Fe-based amorphous magnetic material sample at different magnetic flux values. From Fig. 5, the following three observations can be made:

(i) The feedback coefficient of the upward magnetization changes with both the magnitude of magnetic flux density and magnetic field strength;
(ii) Near to the coercive force, the feedback coefficient jumps to the opposite direction and then decreases exponentially with the magnetic field strength; and
(iii) The value of feedback coefficient decreases with the increase of flux density magnitude.

It is reported in [15] that the higher the standard deviation of dM/dH, the higher error is likely in the calculated results, and the standard deviation of dM/dH in the region near the coercive forces is higher than that of the rest part of B-H loop. Accordingly, from Fig. 6, it can be observed that at the vicinity of coercive forces, the discrepancy between the simulated and measured B-H loops is higher than the other part of the loop. To reduce the discrepancy, a new technique is proposed to identify the feedback coefficient. On the upward trajectory, K is taken as a positive value for $H \geq H_c$ and a negative value for $H < H_c$. At the same time, the value of K decreases with the magnitude of magnetic flux density. The values of K at different magnitudes of magnetic flux density (B_m) are calculated in such a way that the hysteresis loss is minimized without distorting the B-H loop, and then the values of K are curve fitted by an exponential function. Fig. 7 shows the feedback coefficient of upward trajectory for $H \geq H_c$ obtained by curve fitting. The feedback coefficients of upward and downward trajectories of Fe-based amorphous magnetic material can be expressed by

$$K = \begin{cases} a_1 e^{-b_1 B_m} + c_1 & H \geq H_c \\ -(a_1 e^{-b_1 B_m} + c_1) & H < H_c \end{cases} \quad \text{(Upward)} \tag{29}$$

$$K = \begin{cases} -(a_1 e^{-b_1 B_m} + c_1) & H \geq -H_c \\ (a_1 e^{-b_1 B_m} + c_1) & H < -H_c \end{cases} \quad \text{(Downward)} \tag{30}$$

where a_1=1.40113×10^{-4}, b_1=4.71577, and c_1=2.95626×10^{-7}, respectively. The proposed generalized Preisach model with the proposed feedback coefficient, however, can effectively reduce the discrepancy between the simulated and experimental results, as shown in Fig. 6.

Magnetization using the generalized Preisach model can be calculated by (12) where the first term is calculated by the normal Preisach model and the value of squareness, and the rest is calculated from the anhysteretic magnetization and squareness. The resultant magnetization is calculated iteratively until the error between two

successive results meets a prespecified convergence criterion. To increase the convergence rate, a suitable acceleration factor or relaxation coefficient, g, is used, and magnetization in each iteration is updated as follows

$$M_o' = M_o + g\left(M - M_o\right) \tag{31}$$

where M_o', M and M_o are the updated, current and previous magnetizations, respectively.

Minor loops occur due to the incremental H and B, and hence the applied H contains local reversible points. To extract the simulated magnetic flux density using the Preisach model, the local reversible points must be popped out if the operating magnetic field strength outstrips the last reversible point in the previous opposite trajectory [22]. Consequently, the minor loop is wiped out and does not affect the next step magnetization process. Fig. 8 shows an applied magnetic field which contains two pairs of local reversible points (b, c, e and f). The general magnetization process is carried out up to the popping out point, P. When the operating magnetic field strength exceeds the value of magnetic field strength at point P which is equal to the magnetic field strength at point b, the last reversible magnetic field strength H_{cc} (magnetic field strength at point c) is replaced by H_a (magnetic field strength at reversible point a) in the magnetization process. As a result, the minor loop is completed, and the magnetization process proceeds onto the major B-H loop. Due to the minor loops, the loss in the core increases.

5. Implementation of Inverse Preisach Models

5.1. Implementation of the Normal Inverse Preisach Model

The normal inverse Preisach model also uses the limiting loop as the input data. The corresponding derivative of upward and downward magnetizations with respect to the magnetic field strength H are then calculated. The derivative of Preisach function can be calculated in two ways: the first one is to use the derivatives obtained by (20) or (21) depending on the sign of H, and the other is to calculate it numerically from the data table of Preisach function.

On the initial magnetization curve, the derivative of magnetisation with respect to H (dM/dH) is calculated by (19), and $H(t)$ is then calculated by (13) and (14). Just like the normal Preisach model, the process continues until it reaches the first reversible point. The magnetic field strength at a reversible point and its corresponding magnetization is stored in a stack. After that the derivative of magnetization with respect to H is calculated by (15) and (17) for the downward trajectory. Similarly, (16) and (18) can be used to calculate the derivative of magnetization with respect to H on the upward trajectory. The magnetic field strength is then calculated from dM/dH by (13) and (14). The process is repeated until it reaches the final time step.

5.2. Implementation of Generalized Inverse Preisach Model

Due to consideration of the reversible magnetization and feedback coefficient in the proposed generalized inverse Preisach model, the calculation of dB/dH becomes different from the normal inverse Preisach model as shown in (26). The dM/dH_e in (26) is calculated by (25) which requires the normal Preisach model, squareness, and data table of dM_{anh}/dH_e. The other process is then done like the normal inverse Preisach model. The normal inverse Preisach model produces a higher error than the normal Preisach model as shown in Tables 2 and 3 (Section *7.2.*), since $H(t)$ is calculated by (10) which is a successive approximation procedure neglecting the higher order derivative terms. Therefore, the feedback coefficient for the generalized inverse Preisach model is considered slightly higher than the generalized Preisach model as shown in Fig. 7 to compensate the excess error. The value of c_1 in (29) and (30) is increased from 2.95626×10^{-7} to 9.305626×10^{-7}, and the other values of parameters are the same as those in the generalized Preisach model. The flow chart of the generalized inverse Preisach model is shown in Fig. 9.

Just like the generalized Preisach model, the generalized inverse Preisach model requires modification during wiping out of minor loops. When the magnetic flux density outstrips the popping point as shown in Fig. 8, the local reversible magnetic field strength is replaced by the global reversible magnetic field strength like the generalized Preisach model. After wiping out the minor loop, the rest process is carried out as the generalized inverse Preisach model. Since the feedback coefficient is calculated from a major loop, the feedback coefficient in this case is only applied on the major loop.

6. Incorporation of Dynamic Effects

The abovementioned models can only predict the static hysteresis loss. If the excitation frequency increases, the other core loss components, such as the eddy current and excess losses, which are also known as dynamic losses, have to be considered for calculating the total core loss. According to the domain model, the eddy current losses are produced by micro-eddy currents induced at the vicinity of moving domain walls as shown in Fig. 10 (a) [22, 30]. Since the ribbon of amorphous magnetic material is very thin, the total eddy current loss is

significantly smaller than those in silicon steel sheets. For simplicity, in the low and medium frequency range, the eddy current paths can be considered as global as shown in Fig. 10 (b), which is known as the classical eddy current model. Thus, the magnetic field strength due to the eddy current according to the classical model can be obtained by [10]

$$H_{eddy} = \frac{\sigma d^2}{12}\frac{\Delta B}{\Delta t} \tag{32}$$

where σ and d are the conductivity and thickness of the amorphous ribbon, respectively, and ΔB is the change of magnetic flux density between two successive discrete time steps.

Similarly, the magnetic field strength corresponding to the excess loss can be expressed by [10,11]

$$H_{exc} = \sqrt{\sigma G V_0 A_l}\,\frac{\Delta B}{\Delta t^{0.5}\left|\Delta B\right|^{0.5}} = K_{exc}\,\frac{\Delta B}{\Delta t^{0.5}\left|\Delta B\right|^{0.5}} \tag{33}$$

where A_l is the cross-sectional area of the ribbon, G and V_0 are constant coefficients depending on the material metallurgical properties, and K_{exc} is equal to the square root of the product of A_l, G, V_0 and σ.

6.1. Identification of Dynamic Coefficients

While the eddy loss parameters (σ and d) can be readily measured or from the data sheet provided by manufactures, the measurement of excess loss coefficients A_l, G and V_0 are very difficult**.** Instead, K_{exc}, which is the square root of the product of A_l, G, V_0 and σ, can be calculated directly from the core losses per unit volume per Hz measured under sinusoidal excitations of different frequencies (starting form 1 Hz or less than 1 Hz) with the same magnetic flux density by curve fitting the data by [11]

$$P_t = P_h + \frac{\sigma\pi^2 d^2}{6}B_m^2 f + 8.76K_{exc}B_m^{1.5}f^{0.5} \tag{34}$$

where P_t is the total core loss per unit volume per Hz, and the first, second and third terms on the right hand side are the hysteresis (P_h), eddy current and excess losses per unit volume per Hz, respectively.

To achieve a higher accuracy, the procedure can be repeated for different flux densities and the average K_{exc} is finally calculated.

6.2. Implementation of Generalized Inverse Preisach Dynamic Hysteresis Model

To incorporate the dynamic effects into the generalized inverse Preisach model, the magnetic field strength related to the static hysteresis loss is firstly calculated by the generalized inverse Preisach model, and the magnetic field strengths corresponding to the eddy current and excess losses are then calculated by (32) and (33), respectively. The total magnetic field strength is finally obtained by summing up all these components of magnetic field strength.

7. Experimental Verification

7.1. Experimental Testing Method

This section presents the experimental verification of the proposed generalized inverse Preisach model of dynamic hysteresis and comparisons between the proposed and the normal Preisach models.

Fig. 11 shows a test platform for measuring the hysteresis effects of Fe-based amorphous material samples set up based on [31] and [32]. The ring core sample, which is obtained from Guangzhou Amorphous Electronic Technology Co. Ltd., China [33], is wound with two coils of equal number of turns, known as the excitation and search coils, respectively. Table 1 lists the dimensions of different core samples and number of turns of the coils. The Labview software is utilized for excitation specification and data acquisition. A power amplifier is utilized to control both the excitation voltage and power levels. The excitation current is worked out by measuring the voltage drop (v_{R}) across a resistor of 1 **Ω**, which is connected in series with the excitation coil. Similarly, the magnetic flux density is derived by measuring the induced electromotive force (*emf*) in the search coil. The measured data are stored in XLS files and processed by a MATLAB program.

The magnetic field strength is obtained from the excitation current by

$$H(t) = \frac{N_{ex}i_{ex}(t)}{l_m} \tag{35}$$

where i_{ex} is the excitation current, l_m the mean length of magnetic core, and N_{ex} the number of turns of excitation coil.

The magnetic flux density is calculated by integrating the induced *emf* in the search coil with respect to time by

$$B(t) = \frac{1}{N_s A}\int v_s(t)dt \tag{36}$$

where A is the effective cross-sectional area of magnetic core, v_s the induced *emf*, and N_s the number of turns of search coil.

Finally, the core loss per unit volume per Hz (P) can be calculated by

$$P = \int_T H\frac{dB}{dt} \tag{37}$$

For minor loops, a voltage of 1 Hz fundamental sinusoidal component with a third harmonic component is used as the excitation voltage. A proportional integral controller is also integrated with the experimental set up to control the size and position of the minor loops. Fig. 12 shows an experimental *B-H* loop which contains two minor loops over a major loop.

7.2. Verification of Simulated Results

As shown in Fig. 3 (Section *4.1.*), the calculated and measured magnetic flux densities for a given magnetic field strength waveform are in close agreement. Table 2 tabulates the comparison of hysteresis losses at different magnetic flux densities obtained by the normal and generalized Preisach models and experimental measurement. From Table 2, the following three important observations can be made:

(i) The calculated and measured losses are very close to each other although the discrepancy increases at a low magnetic flux density since the magnetic coercive force at low flux density is significantly smaller than that of the limiting loop.
(ii) The generalized Preisach model provides a significantly higher precision in calculating the hysteresis loss than that of the normal Preisach model, especially at low magnetic flux densities.
(iii) The hysteresis loss calculated by the proposed feedback coefficient has lower error at a low magnetic flux density than that obtained by the constant feedback coefficient. This can also be seen from Fig. 6 that at the vicinity of H_c, the magnetic flux density calculated by using the proposed feedback coefficient is closer to the experimental result than that obtained by using constant feedback coefficient (K= -1.29113×10^{-6}).

Similar to Table 2, Table 3 shows a comparison of the hysteresis losses at different magnetic flux densities obtained by the inverse Preisach models with the measured results. From Table 3, the following three observations can be made:

(i) The generalized inverse Preisach model with the proposed feedback coefficient shows better agreement with the measured results than the normal inverse Preisach model and generalized inverse Preisach model with constant feedback coefficient.
(ii) The error decreases with the increase of magnetic flux density.
(iii) The calculation of maximum magnetic field strength by both inverse Preisach models are almost the same, and both are close to the measure result. For instance, the calculated maximum magnetic field strength by the normal and proposed inverse Preisach models at 1.26 T are 76.95 A/m and 75.83 A/m, respectively, whereas the measured magnetic field strength is 78.19 A/m.

Furthermore, the prediction accuracies of hysteresis loss of both the normal and inversed Preisach models depend significantly on the number of sampling points of magnetic flux density per cycle. For instance, if the number of sampling points of magnetic flux density per cycle is increased from 500 to 1000, the error of hysteresis loss calculation at 1.18 T can be reduced from 8.50% to 5.88%.

When the minor loops are considered over a major loop, the discrepancy between the calculated and experimental results increases slightly as shown in Figs. 8 and 12 due to the following reasons: (i) the congruent property of the normal Preisach model, although for the generalized Preisach model the congruent property has been relaxed [16]; (ii) the low incremental magnetic field strength as the discrepancy between the calculated and experimental results increases at low magnetic field strength [28]; (iii) further deviation occurs if the minor loops happen at the vicinity of magnetic coercive force for the reason discussed in Section 4.2.2. However, a significant improvement in the calculation of hysteresis loss is obtained by the proposed inverse Preisach model in comparison to the normal inverse Preisach model. Table 4 presents a comparison of the calculated and measured hysteresis losses with minor loops. As shown, the errors in the calculation of hysteresis loss at 1.24 T by the proposed and the normal inverse Preisach models are 7.24% and 11.55%, respectively.

In the case of dynamic hysteresis losses, the losses are calculated by the normal and proposed inverse Preisach models at the same flux density magnitude with different frequencies. The calculated and experimental results are then curve fitted and compared with each other as shown in Fig. 13. As shown, the results calculated by the proposed generalized inverse Preisach model are closer to the measured results than those by the normal Preisach model.

The experimental and calculated *B-H* loops of the Fe-based amorphous magnetic material at 500 Hz are shown in Fig. 14. As shown, the calculated *B-H* loop by the proposed model is very close to the measured loop. However, the *B-H* loop becomes smaller when the excess loss is excluded from the core loss. On the other hand, when both the eddy current and excess losses are excluded, i.e. if only hysteresis loss is considered, the *B-H* loop seems similar to the loop that considers both hysteresis and eddy current losses. The reason for this similarity is that the effects of eddy current loss in the amorphous sample are not as significant as those in the conventional magnetic materials, e.g. SiFe sheets, since the thickness of the ribbon of Fe-based amorphous magnetic material sample is much thinner than those of SiFe sheets [34].

8. Conclusion

A generalized inverse Preisach dynamic hysteresis model is proposed in this paper for characterization of Fe-based amorphous magnetic materials. The proposed model incorporates the reversible magnetization component in the Preisach elemental operator and magnetization dependent feedback coefficient that are missing in the existing types of inverse Preisach models and thus can accurately characterize the dynamic performance of magnetic cores of Fe-based amorphous magnetic materials for both low and middle frequency applications. The theoretical derivation and numerical implementation of the proposed model are presented in detail based on discussions of the existing normal Presiach model, generalized Preisach model, and normal inverse Preisach model. The theoretical results of the proposed and existing inverse Preisach models are compared with the experimental measurement results. The proposed model has demonstrated higher accuracy than the normal inverse Preisach model for the cases of both major loops and major loop plus minor loops under different excitation magnitudes as well as frequencies. In future, the proposed model will be integrated into a finite element solver for conducting more sophisticated electromagnetic analyses by considering the strong nonlinear dynamic magnetic hysteresis effects.

Reference

[1] P. C. Sarker, M. R. Islam, Y. Guo, J. Zhu, H. Y. Lu, State-of-the-art technologies for development of high frequency transformers with advanced magnetic materials, *IEEE Trans. Appl. Supercond.* vol. 29 (2) (2019) Art. 7000111.

[2] M. A. Bahmani, Design and optimization considerations of medium-frequency power transformers in high-power DC-DC applications, Ph.D. Dissertation, Dept. Energy Environ., Chalmers Univ. Technol., Sweden 2016.

[3] M. R. Islam, K. M. Muttaqi, D. Sutanto, J. Zhu, Design and implementation of amorphous magnetic material common magnetic bus for the replacement of common dc bus, IEEE Trans. Magn. vol. 54 (11) (2018) Art. 2002004.

[4] Metglas, Magnetic Alloy, Technical Bulletin. Available: https://metglas.com/ (Accessed 10 July 2018).

[5] Henan ZY Amorphous Technology Co. Ltd. Available: https://www.zyamorphous.com/. (Accessed 25 September 2019).

[6] S. Barg, K. Ammous, H. Mejbri, A. Ammous, An improved empirical formulation for magnetic core losses estimation under nonsinusoidal induction, *IEEE Trans. Power Electron.* vol. 32 (3) (2017) 2146–2154.

[7] M. R. Islam, G. Lei, Y. Guo, J. Zhu, Optimal design of high-frequency magnetic links for power converters used in grid-connected renewable energy systems, IEEE Trans. Magn.vol. 50 (11) (2014) Art. 2006204.

[8] A. Benabou, J. V. Leite, S. Clénet, C. Simão, N. Sadowski, Minor loops modelling with a modified Jiles–Atherton model and comparison with the Preisach model, J. Magn. Magn. Mater. vol. 320 (20) (2008) 1034–1038.

[9] Y. Li, L. Zhu, J. Zhu, Core loss calculation based on finite-element method with Jiles–Atherton dynamic hysteresis model, IEEE Trans. Magn. vol. 54 (3) (2008) Art. 1300105.

[10] N. Sadowski, N. J. Batistela, J. P. A. Bastos, M. Lajoie-Mazenc, An inverse Jiles-Atherton model to take into account hysteresis in time-stepping finite-element calculations, IEEE Trans. Magn. vol. 38 (2) (2002) 797–800.

[11] E. Fallah, J. S. Moghani, A new approach for finite-element modeling of hysteresis and dynamic effects, IEEE Trans. Magn. vol. 42 (11) (2006) 3674–3681.

[12] A. Benabou, S. Clénet, F. Piriou, Comparison of Preisach and Jiles–Atherton models to take into account hysteresis phenomenon for finite element analysis, J. Magn. Magn. Mater. vol. 261 (1) (2003) 139–160.

[13] G. Kadar, E. D. Torre, Hysteresis modeling: I. Non-congruency, IEEE Trans. Magn. vol. 23 (5) (1987) 2820–2822.

[14] E. D. Torre, Existence of magnetization-dependent Preisach models, IEEE Trans. Magn. vol. 27 (4) (1991) 3697–3699.

[15] J. Oti, F. Vajda, E. D. Torre, Identification of parameters in a moving model, J. Appl. Phys. vol. 69 (8) (1991) 4826–4828.

[16] F. Vajda, E. Della Torre, Efficient numerical implementation of complete-moving-hysteresis models, IEEE Trans. Magn. vol. 29 (2) (1993) 1532–1537.

[17] I. D. Mayergoyz, Mathematical Models of Hysteresis, Springer-Verlag, New York, 1991.

[18] Z. Szabó, J. Füzi, Implementation and identification of Preisach type hysteresis models with Everett Function in closed form, J. Magn. Magn. Mater. vol. 406 (2016) 251–258.

[19] Y. Cao, K. Xu, W. Jiang, T. Droubay, P. Ramuhalli, D. Edwards, B. R. Johnson, J. McCloy, Hysteresis in single and polycrystalline iron thin films: major and minor loops, first order reversal curves, and Preisach modeling, J. Magn. Magn. Mater. vol. 395 (2015) 361–375.

[20] D. Atherton, B. Szpunar, J. Szpunar, A new approach to Preisach diagrams, IEEE Trans. Magn. vol. 23 (3) (1987) 1856–1865.

[21] E. D. Torre and G. Kadar, Hysteresis modeling: II. Accommodation, IEEE Trans. Magn. vol. 23 (5) (1987) 2823–2825.

[22] J. G. Zhu, Numerical modelling of magnetic materials for computer aided design of electromagnetic devices, Ph.D. Dissertation, School of Electrical Engineering, University of Technology Sydney, Australia, July 1994.
[23] I. D. Mayergoyz, Dynamic Preisach models of hysteresis, IEEE Trans. Magn. vol. 24 (6) (1988) 2925–2927.
[24] Y. Bernard, E. Mendes, F. Bouillault, Dynamic hysteresis modeling based on Preisach model, IEEE Trans. Magn. vol. 38 (2) (2002) 885–888.
[25] E. Cardelli, E. D. Torre, B. Tellini, Direct and inverse Preisach modeling of soft materials, IEEE Trans. Magn. vol. 36 (4) (2000) 1267–1271.
[26] L. R. Dupré, R. V. Keer, J. A. A. Melkebeek, Evaluation of magnetostrictive effects in soft magnetic materials using the Preisach theory, J. Magn. Magn. Mater. vol. 254–255 (2003) 121–123.
[27] S. Y. R. Hui, J. Zhu, Numerical modelling and simulation of hysteresis effects in magnetic cores using transmission-line modelling and the Preisach theory, IEE Proc. – Elect. Pow. Appls. vol. 142 (1) (1995) 57–62.
[28] S. R. Naidu, Simulation of the hysteresis phenomenon using Preisach's theory, IEE Proc. A Phy. Sci. Mea. Inst. Man. Edu. vol. 137 (2) (1990) 73–79.
[29] S. Talebian, Y. Hojjat, M. Ghodsi, M. R. Karafi, S. Mirzamohammadi, A combined Preisach–hyperbolic tangent model for magnetic hysteresis of Terfenol-D, J. Magn. Magn. Mater. vol. 396 (2015) 38–47.
[30] C. R. Boon and J. A. Robey, Effect of domain-wall motion on power loss in grain-oriented silicon-iron sheet, Proc. IEE. vol. 115 (10) (1968) 1535–1540.
[31] P. Kis, M. Kuczmann, J. Fuzi, A. Ivanyi, Hysteresis measurement in LabView, Pysica B: Cond. Matt. vol. 343 (2004) 357–363.
[32] S. Y. R. Hui, J. G. Zhu, V. S. Ramsden, A generalized dynamic circuit model of magnetic cores for low- and high-frequency applications. II. Circuit model formulation and implementation, IEEE Trans. Power Electron. vol. 11 (2) (1996) 251–259.
[33] Guangzhou Amorphous Electronic Technology Co. Ltd. [Online]. Available: https://www.coilcore.com/. (Accessed 22 December 2019)
[34] A. Krings, M. Cossale, A. Tenconi, J. Soulard, A. Cavagnino, and A. Boglietti, Magnetic materials used in electrical machines: a comparison and selection guide for early machine design, IEEE Ind. Appl. Mag. vol 23 (6) (2017) 21–28.

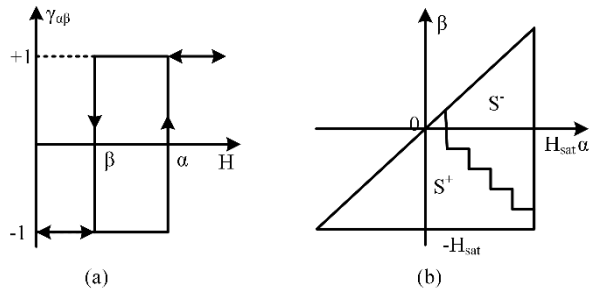

Fig. 1. (a) Rectangular hysteresis model of magnetic dipoles [27,29], and (b) Preisach diagram [27].

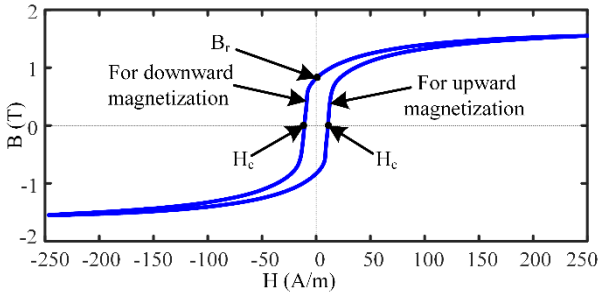

Fig. 2. Limiting loop of Fe-based amorphous magnetic material.

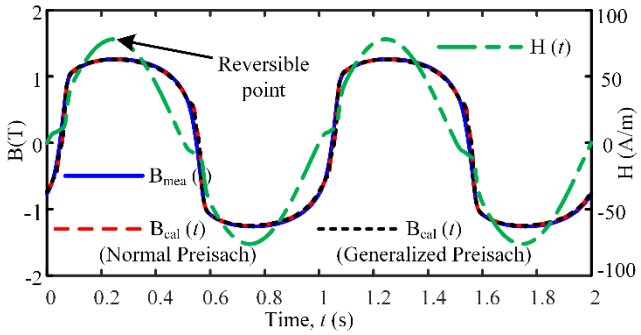

Fig. 3. Applied magnetic field strength and corresponding measured and calculated magnetic flux densities.

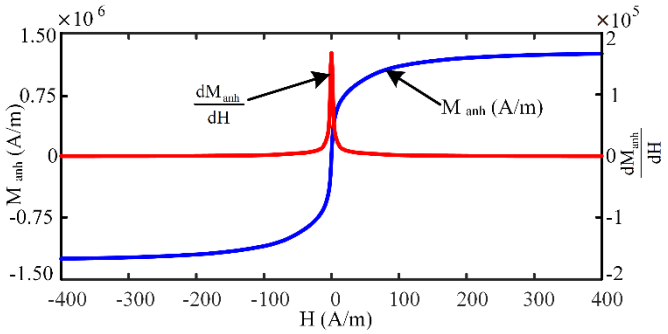

Fig. 4. Anhysteretic magnetization curve of Fe-based amorphous magnetic material calculated by the normal Preisach model and its derivative with respect to magnetic field strength H.

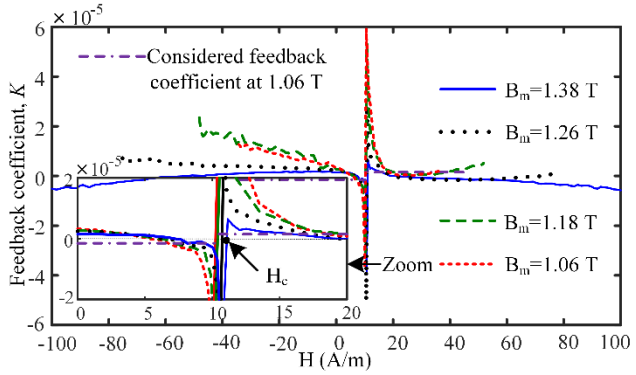

Fig. 5. Feedback coefficient for the upward magnetization of Fe-based amorphous magnetic material at different magnetic flux magnitudes.

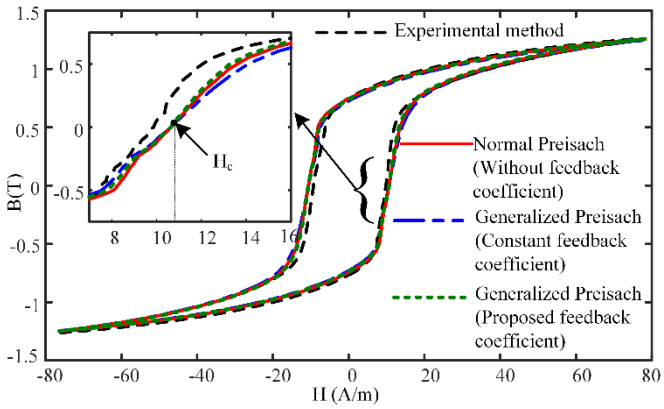

Fig. 6. Comparison of the B-H loops predicted by using constant feedback coefficient, proposed feedback coefficient, and no feedback coefficient with the experimental result.

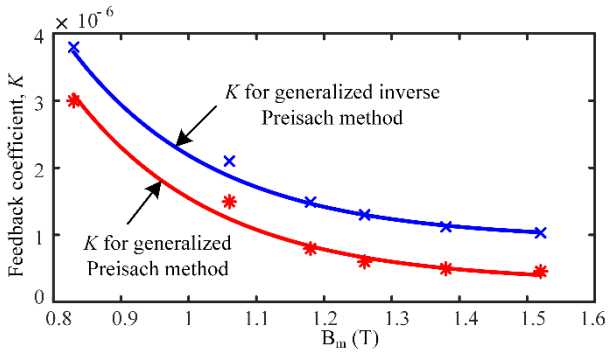

Fig. 7. The feedback coefficient of upward magnetization for $H \geq H_c$.

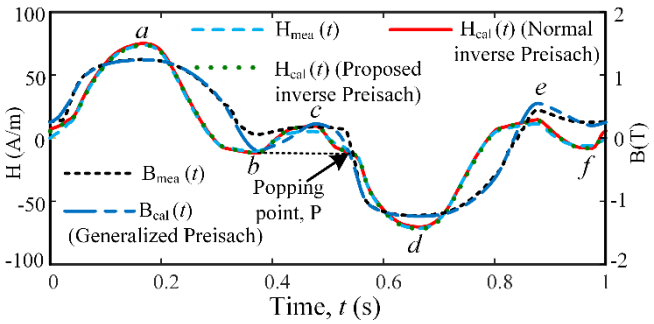

Fig. 8. Calculated and measured magnetic field strengths and magnetic flux densities for minor loops.

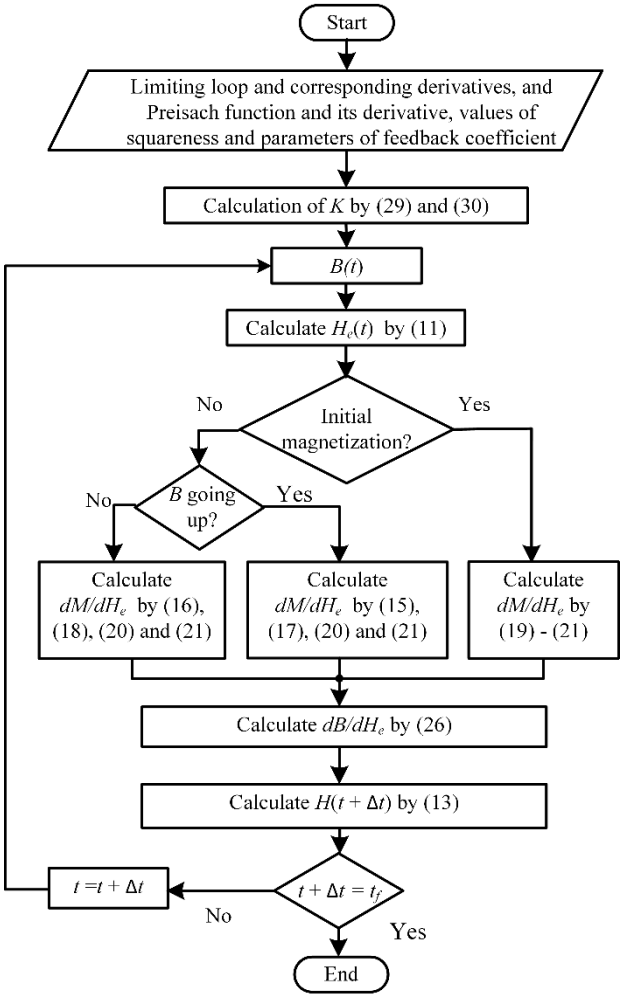

Fig. 9. Flow chart of the proposed inverse Preisach model.

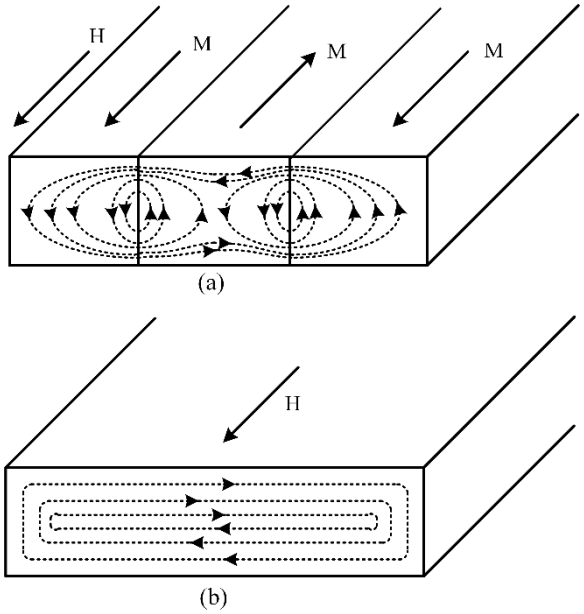

Fig. 10. The eddy current paths in the ribbon of a magnetic material, (a) domain model [22, 30], and (b) classical model [22, 30].

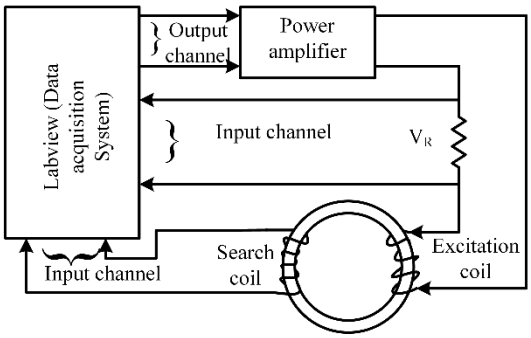

Fig. 11. Experimental set up for measuring *B-H* loops.

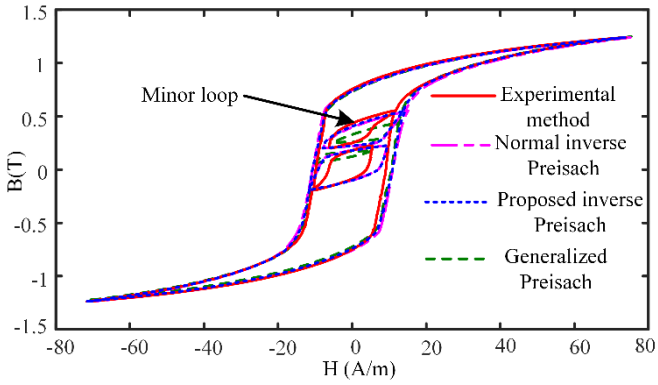

Fig. 12. Comparison among measured and calculated *B-H* loops where minor loops are considered over a major loop.

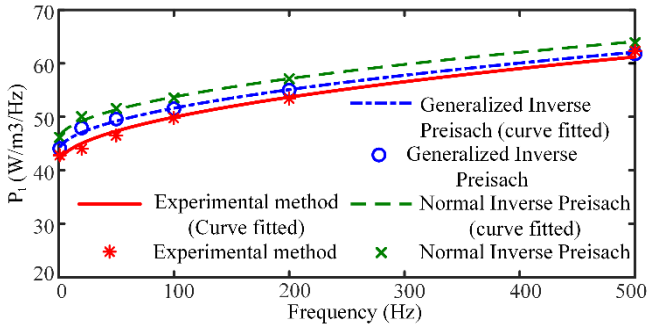

Fig. 13. A comparison between calculated and measured core losses versus frequency at B_m=1.29 T by the proposed and normal inverse Preisach models.

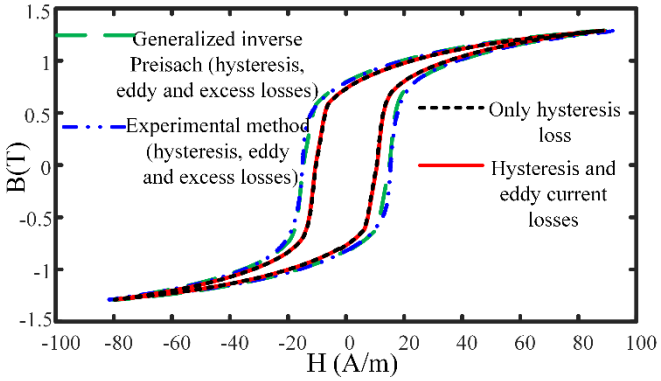

Fig. 14. Calculated and measured *B-H* loops at 500 Hz and 1.29 T.

Table 1
Different Parameters of Tested Core

Parameters	Values
Material name	Fe-based amorphous(j1k101) [5,32]
Core type	Toroidal
Thickness (mm)	0.023 ~ 0.026
Height (mm)	30
Outer diameter (mm)	63
Inner diameter (mm)	45
Stacking factor	0.80
Mass density (kg/m3)	7180
Resistivity μΩ.cm	130
Number of turns of coils	24/24

Table 2
Comparison of Calculated and Measured Hysteresis Loss for Preisach Models

B_m (T)	Test	Normal Preisach		Generalized Preisach			
				Proposed K (B_m)		*Constant K*	
	P_h (W/ m^3/Hz)	P_h (W/ m^3/Hz)	*Error* (%)	P_h (W/ m^3/Hz)	*Error* (%)	P_h (W/ m^3/Hz)	*Error* (%)
0.83	21.00	28.40	35.24	26.13	24.43	27.73	32.05
1.06	31.24	33.51	7.27	32.12	2.82	32.76	4.87
1.18	37.41	38.03	1.66	37.24	-0.45	37.51	0.27
1.26	42.52	43.30	1.83	41.98	-1.27	42.48	-0.09
1.38	50.38	51.40	2.02	50.09	-0.57	50.56	0.36
1.52	63.22	66.14	4.62	64.64	2.25	65.51	3.62

Table 3
Comparison of calculated and measured hysteresis loss for inverse Preisach models

B_m (T)	Test	Normal inverse Preisach		Generalized inverse Preisach			
				Proposed K		*Constant K*	
	P_h (W/m^3/Hz)	P_h (W/m^3/Hz)	*Error* (%)	P_h (W/m^3/Hz)	*Error* (%)	P_h (W/m^3/Hz)	*Error* (%)
0.83	21.00	27.21	29.57	25.12	19.62	27.16	29.33
1.06	31.24	35.76	14.47	34.03	8.93	35.75	14.44
1.18	37.41	41.54	11.04	39.61	5.88	41.50	10.93
1.26	42.52	44.88	5.55	42.89	0.87	44.71	5.15
1.38	50.38	51.09	1.41	48.72	-3.29	50.95	1.13
1.52	63.22	67.64	6.99	63.94	1.34	67.41	6.62

Table 4
Comparison of calculated and measured hysteresis loss with minor loops

P_h (Test) (W/m^3/Hz)	Normal inverse Preisach		Generalized inverse Preisach	
	P_h (W/m^3/Hz)	*Error*	P_h (W/m^3/Hz)	*Error*
46.67	52.06	11.55%	50.05	7.24%